PVDF/$BaTiO_3$/Carbon Nanotubes Ternary Nanocomposites Prepared by Ball Milling: Piezo and Dielectric Responses

J. González-Benito[1*], D. Olmos[1], J.M. Martínez-Tarifa[2], G. Gonzalez-Gaitano[3], F.A. Sanchez[4]

[1]Dpt. Materials Science and Engineering, IQMAAB, Universidad Carlos III de Madrid.
[2]Dpt. Electric Engineering. Universidad Carlos III de Madrid.
[3]Dpt. Chemistry. Universidad de Navarra
[4]Universidad Nacional Autónoma de Nicaragua.

Correspondence to: Javier González-Benito (E-mail: javid@ing.uc3m.es)

ABSTRACT

Nanocomposites based on poly(vinylidene fluoride), PVDF, filled with $BaTiO_3$ particles, BT, and multi-walled carbon nanotubes, MWCNT, were prepared by high energy ball milling, HEBM and subsequent hot pressing. This method of materials preparation allowed obtaining uniform dispersions of the nanofillers. The influence of the particles on the polymer structure and morphology was studied. To understand the origin of changes in the PVDF properties, thermal and electrical behaviors of the PVDF/$BaTiO_3$/MWCNT nanocomposites were studied as a function of composition. The addition of $BaTiO_3$, MWCNT or its mixture had not any influence on the PVDF polymorphism. However, calorimetric results pointed out that the presence of the nanofillers exerted nucleation mainly ascribed to the surface to volume ratio of the nanoparticles. The capacitance of the composites increased as the nanofiller content increased, being the effect also mainly dependent on the surface to volume ratio of the nanoparticles. The dielectric behavior of the materials as a function of frequency was modeled by a Debye equivalent circuit only below the percolation threshold respect to the amount of MWCNT. The piezoelectric behavior of the ternary nanocomposites was highly affected by the incorporation of the nanofillers only when high dielectric losses occurred above the percolation threshold.

INTRODUCTION

In the last two decades easy processing and low cost materials with special electrical properties are receiving special attention. In particular, thermoplastics with high dielectric constant, k, and low dielectric losses gather those characteristics, making them good candidates to fabricate, among others, electric energy storage devices, capacitors, etc. However, most of the thermoplastic polymers have low dielectric constant so their modification might be a good choice to overcome this lack without affecting other properties. In this sense, a common approach is the addition of high dielectric constant ceramic fillers to the polymeric matrix [1] . However, some investigations pointed out that only significant

increase of permittivity can be achieved with the use of important loads of ceramic filler (more than 40% v/v) [2,3] which might compromise other important properties of the material for its proper performance. Therefore, other approaches should be investigated as, for example, the addition of a third phase which allows enhancing synergy at low loads of the ceramic filler.

In general, when polymers are loaded with conductive particles near the percolation threshold their dielectric constant increase [4–10]. These dielectric changes are mainly a consequence of the important increase of interfacial polarization. Looking for new ways of tuning dielectric properties of polymers an interesting option might be to fill polymers with a combination of high k dielectric particles (i.e. barium titanate) and conductive particles (i.e. graphene, carbon nanotubes or carbon nanofibers). Besides, if high charge accumulation is expected, the use of nanofillers should be favorable due to the possibility of creating a large interface region where charge might be located after applying the corresponding electric field.

From a physical point of view, it is reasonable to think that if a uniform dispersion of conductive nanoparticles is achieved, nano or microcapacitors can be formed within the polymer matrix. This idea is used to understand the abrupt increase of the dielectric constant in a polymer based nanocomposite when the volume fraction of conductive nanofiller is close to the percolation threshold [11,12]. Due to this, carbon nanotubes (CNT), with superior electrical and thermal conductivity values, might be an excellent choice to enhance the permittivity of this sort of composites. In fact, CNT allow much lower percolation threshold in composites than conventional spherical fillers since their high aspect ratio facilitates the formation of conducting networks at much lower volume fraction. Besides, CNT present extremely high mechanical strength, which can prevent possible losses in the mechanical properties of the polymer matrix induced by the presence of ceramic particles. On the other hand, the addition of different kind of fillers into a crystalline polymer matrix may affect not only the conformation and morphology of the polymer, but also its crystalline structure, the process of spherulites formation and the crystallization rate [13–18]. Therefore, when considering systems with more than one filler, it is necessary to understand the influence of their joint presence on: i) the final properties of the composite and ii) whether the changes appear due to the sole presence of the fillers or because of an induced modification of the polymer structure and/or morphology.

Because of its good piezoelectric and pyroelectric properties, Poly(vinylidene fluoride), PVDF, a semicrystalline polymer, is being used to make sensors, actuators and transducers. Besides, due to its good mechanical strength and high stability to moisture, chemicals, abrasion and intense radiation, this polymer have many advantages over traditional ceramic electroactive materials [19]. Four crystalline phases, α, β, γ and δ [20,21] are mainly indentified in PVDF, being the α phase (the most stable) and the β phase (the most polar with the most important piezo- and pyro-electric responses) the most used and studied [22,23]. Some results point out that mechanical and thermal properties of neat PVDF do not seem adequate for certain needs in extraterrestrial environments [24,25]. Hence, great efforts should be focused on improving these properties in addition to the above mentioned electrical properties. In several researches ferroelectric ceramic particles such as $BaTiO_3$ [26], $PbTiO_3$ [27,28] and $PbZrTiO_3$ [29,30] have been chosen to be embedded in polymers as fillers to form 0–3 type composites. In particular,

special attention has received the possibility of increasing the permittivity of PVDF films by the incorporation of nanoparticles due to its potentiality in energy storage applications [31–40].

On the other hand, CNT reinforced PVDF nanocomposites have shown improvements in the mechanical, thermal, and electrical properties compared to the neat PVDF [41]. Recent studies about PVDF/CNT nanocomposites indicate that when adding CNT to PVDF, appearance of β-phase can be induced [41]. Besides, CNT may act as nucleating agents exerting a crystallization confinement in the PVDF that depends on the nanotubes concentration [42,43]. However, a clear explanation of the origin of those changes has not been given yet, being the answer to that question even more difficult when a second filler is added to the polymer matrix. To the best of our knowledge, not much work has been done in relation to PVDF nanocomposites prepared by the addition two types of nanofillers.

An important consideration when dealing with these systems is that, in order to achieve the best performance of them, a uniform dispersion of the particles is required. The presence of agglomerates may lead to non-desired electrical or mechanical properties. This challenge is particularly difficult when carbon nanotubes are used since they tend to self-aggregate because of intense Van der Waals attractions. There have been quite strategies to achieve efficient dispersions of nanoparticles in different matrices, for example, modification of the nanoparticles surface [44–46]; "in situ" polymerization by prior dispersion of the nanoparticles in a monomer [47], and addition of surfactants or other dispersant substances [48]. However, none of them seems to ensure a uniform dispersion of the nanofiller in polymer matrices when the amount of it is higher than 5% by weight or when the polymer is highly viscous. Apart from other very difficult methods, some works evidenced that mixing nanoparticles with polymers by the use of high energy ball milling is a good method to attain uniform nanoparticles dispersions within polymers [3,13,14,49–51]. This is mostly due to the strong shear forces imposed by the milling process which allows nanoparticles to be randomly embedded into the polymer [13].

In this work, barium titanate particles, $BaTiO_3$ having less than 300 nanometers of diameter and multiwall carbon nanotubes, MWCNT, have been chosen as nanofillers to prepare a series of PVDF/$BaTiO_3$/MWCNT ternary nanocomposites. A two-step process based on an initial mixture by high energy ball milling and subsequent hot pressing was used to obtain materials with uniform dispersion of the nanoparticles. In particular, this study also includes analysis and comparisons in terms of structure and thermal and electrical properties of the composites, in order to understand if the final properties of the composites are due to the sole presence of the particles, the induced structure and morphology variations in the polymer matrix or a combination of both factors.

EXPERIMENTAL

Materials

Poly(vinylidene fluoride), PVDF, was used as the polymer matrix (Sigma-Aldrich; M_n ~ 10,700; M_w ~ 27,500 and density 1.78 g·cm^{-3}). As the fillers multiwall carbon nanotubes, MWCNT, purchased from Sigma-Aldrich (> 95 wt% in carbon, 7.5 nm mean diameter, 5 μm mean length and density 2.1 g/cm^3), and barium titanate submicrometric particles with tetragonal structure

(Curie point 128 ºC) [50], mean diameter 200 nm, 99.9% purity and density 6.02 g/cm^3 (supplied by Nanostructred and amorphous materials) were used.

Sample preparation

Mixtures of PVDF, $BaTiO_3$ and MWCNT with different compositions were prepared. Codes for the samples and relative amount of each component are gathered in Table 1.

Table 1. Codes for the composites prepared and relative amount of each component in them.

Sample	PVDF (% wt)	$BaTiO_3$ (% wt)	MWCNT (% wt)
PVDF	100	0.0	0.0
PVDF-1BT	99.0	1.0	0.0
PVDF-5BT	95.0	5.0	0.0
PVDF-10BT	90.0	10.0	0.0
PVDF-40BT	60.0	40.0	0.0
PVDF-0.1CNT	99.9	0.0	0.1
PVDF-0.5CNT	99.5	0.0	0.5
PVDF-1.0CNT	99.0	0.0	1.0
PVDF-3.0CNT	97.0	0.0	3.0
PVDF-40BT-0.1CNT	59.9	40.0	0.1
PVDF-40BT-0.5CNT	59.5	40.0	0.5
PVDF-40BT-1.0CNT	59.0	40.0	1.0
PVDF-40BT-3.0CNT	57.0	40.0	3.0

Films of the ternary nanocomposites were prepared following several processing steps:

i) PVDF pellets were ground using a MF10 Basic Microfine miller.

ii) Ground PVDF was then blended with $BaTiO_3$ submicrometric particles and MWCNT in different proportions (Table 1) using high energy ball milling, HEBM. The milling was carried out under cryogenic conditions in a RETSCH MM400 apparatus using a stainless steel vessel of 50 cm^3 and 15 stainless steel balls of 9 mm of diameter. About 7 g of mixture were introduced in the vessel and milled at 25 Hz for 1 h using cycles of 5 min of active milling and 15 min of resting in liquid nitrogen to finally obtain a fine powder.

iii) The milled powders were processed by hot pressing (Fontijne TPB374 hot press) to obtain films of thickness ~110 μm (measured with a thickness-meter Easy-Check FN of NEURTEK Instruments with an accuracy of ± 1μm). The powders were then placed between two polished 10×10 cm^2 aluminum plates covered by Kapton® sheets used as anti-adherent material and heated at 200 ºC under a load of 50 kN. Finally, the films were cut to obtain circular specimens used to carry out all tests (Figure 1).

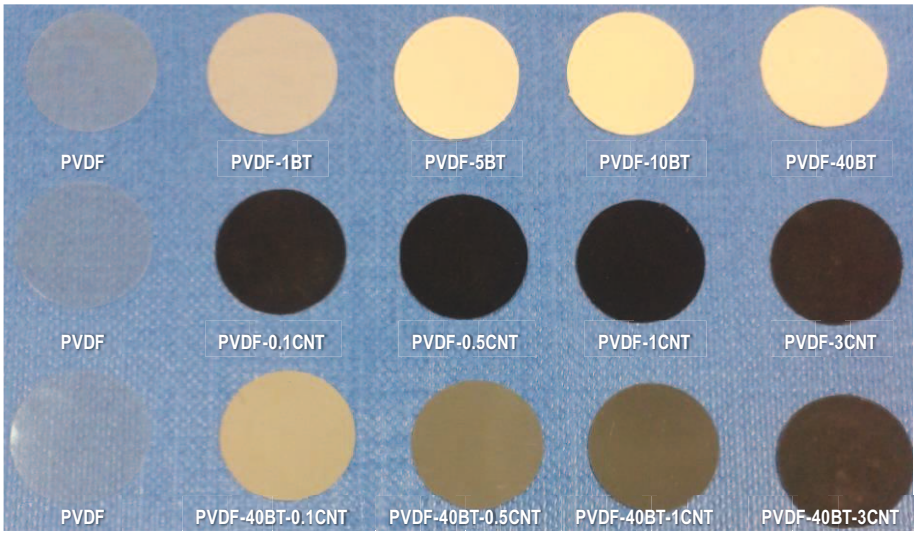

Figure 1. Specimens prepared form films of PVDF containing $BaTiO_3$ and MWCNT (see Table 1 for nomenclature).

Equipments

The nanoparticles dispersion was inspected with a Philips XL30 scanning electron microscope, SEM, using the backscattered electrons, BSE, signal. Microanalysis at specific sites on the surfaces were performed with a DX4i coupled energy-dispersive X-ray spectroscopy (EDAX) detector. To avoid charge accumulation, samples were gold coated by sputtering with a conventional anodic deposition method.

X ray diffraction, XRD, was used to identify and analyze the different crystalline phases in the nanocomposites. Philips X´Pert X ray diffractometer with anti-scattering diffraction slit of 1º, proportional counter and Ni filter and K_α(Cu) radiation of wavelength, λ = 1.54056Å was used. Measurements were carried out at 2θ scanning angles from 10º to 70º.

To study the PVDF structure in the composites Fourier transformed infrared spectroscopy by attenuated total reflectance, FTIR-ATR, was performed using an FTIR Nicolette Avatar 360 spectrometer with a Golden Gate diamond ATR and temperature control. 32 scans per spectrum with a resolution of 4 cm^{-1} were set in all cases.

Dynamic melting and crystallization were studied by differential scanning calorimetry, DSC. The experiments were conducted in non-isothermal mode with a Mettler Toledo 822^e calorimeter under nitrogen atmosphere. To erase the thermal history, samples (2-4 mg) were first heated from 25 to 210ºC at 10ºC/min and then maintained at 220ºC for 10 min. After that, crystallization process was monitored by cooling from 210 to 25ºC at 10ºC/min. Finally, a heating scan from 25 to 210ºC at 10ºC/min was performed to study the melting process.

The crystallization temperatures, T_c, and the enthalpies of crystallization, ΔH_c, were obtained from the DSC exothermic peaks and their integration, respectively, whereas the melting points, T_m, and the enthalpies of fusion, ΔH_m, were obtained from the DSC endothermic peaks and

their integration. To calculate the crystallization degrees, X_c, the following equation was used (eq. 1).

$$X_c = \frac{\frac{(\Delta H_c + \Delta H_m)}{2}}{(1-x)\cdot \Delta H_m^0} \quad (1)$$

where x is the weight fraction of particles and ΔH_m^o is the standard enthalpy of fusion for the fully crystallized PVDF, ΔH_m^o = 104.7 J/g [52].

The electrical tests were carried out using a homemade cell composed of two aluminum circular electrodes with a stem supported by a structure made of two thick sheets of poly methyl methacrylate. The circular speciments were located in between the electrodes and the cell was connected to the equipments through copper cables (Figure 2). After making a small pressure with wing nuts the diameter of the contact area between the samples and electrodes was 10 mm.

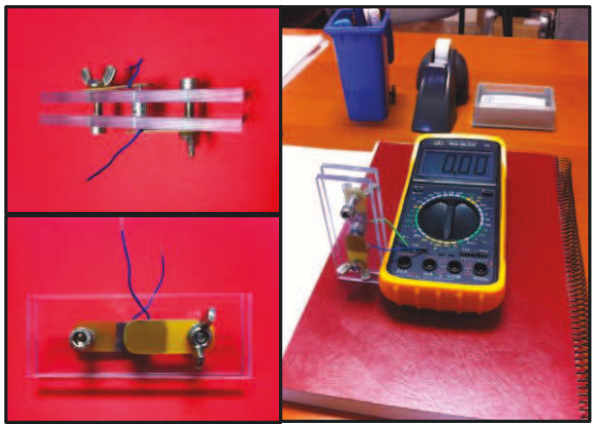

Figure 2. Cell used to carry out the electrical measurements (left) and cell connected to a digital multimeter (right).

The capacitance, C, of the specimens was directly measured using a digital multimeter Mod 60.131 ELECTRO DH and the relative permittivity, ε_r, was deduced from the equation 2:

$$\varepsilon_r = \frac{d}{A\cdot \varepsilon_o}\cdot C \quad (2)$$

Where ε_0 = 8.854 $\times 10^{-12}$ F/m is the permittivity of vacuum, A, the electrode area in contact with the specimen and d the thickness of the specimen.

An impedance analyzer SOLARTRON 1260A was used to carry out the impedance measurements at room temperature in the frequency range 1Hz–1MHz. A 3V sinusoidal voltage signal was applied to the samples and the current was measured to obtain the complex

impedance with its amplitude (ratio between peak voltage and peak current) and phase (phase between voltage and current) as a function of frequency (10 points per decade). The commercial software Zview was used to do the numerical fitting of the impedance data from the use of equivalent circuits.

When a constant electric field, E, is suddenly applied to a dielectric material (a step-function), the resulting polarization, P, may be divided into two parts according to the time scale of the response:

$$P = P_e + P_d \quad (3)$$

Where P_e corresponds to a polarization almost instantaneous due to the displacement of the electrons with respect to the nuclei and P_d is a time-dependent polarization due to the orientation of dipoles under the influence of the electric field [53–56].

On the other hand, for many dielectric materials, the polarization is proportional to the electric field and is related to the relative permittivity, ε_r, as it is described in the following expression:

$$P = \varepsilon_0 \cdot (\varepsilon_r - 1) \cdot E \quad (4)$$

Therefore, from the combination of eqs. 3 and 4 the corresponding contributions to the relative permittivity can be extracted:

$$\varepsilon_{re} = \frac{P_e}{E \cdot \varepsilon_0} + 1 \quad (5)$$

$$\varepsilon_{rd} = \frac{P_d}{E \cdot \varepsilon_0} + 1 \quad (6)$$

On the other hand, in wide frequency ranges and according to the Debye`s model [53], the permittivity ($\varepsilon=\varepsilon_r \varepsilon_0$) is a function of the angular frequency ω (or $2\pi f$ where f is the frequency in Hz) and belongs to the complex domain :

$$\varepsilon_r = \varepsilon_r^{'} - i\,\varepsilon_r^{''} = \varepsilon_{re} + \frac{\varepsilon_{rd} - \varepsilon_{re}}{1 + i\,\omega\,\tau} = \varepsilon_{re} + \frac{\varepsilon_{rd} - \varepsilon_{re}}{1 + \omega^2\,\tau^2} - i\,\frac{\omega\,\tau\,(\varepsilon_{rd} - \varepsilon_{re})}{1 + \omega^2\,\tau^2} \quad (7)$$

Where ε_{re} measures the electronic and atomic resonance polarization of the dielectric, ε_{rd} the ability for the orientation of the permanent dipoles present in the dielectric and τ is the relaxation time, or the time for the dipoles to return to their original position after removing the electrical field [54].

However, impedance is the physical quantity measured as a function of frequency so some expression should be used in order to finally obtain the electrical permittivity. It is well known that the complex impedance can be described by two contributions, Eq. (8) [55].

$Z^* = Z' + iZ''$ (8)

where Z' and Z'' are the real and imaginary parts of the complex impedance. The polarization of the dielectrics under consideration is proposed to be modeled by a RC circuit connected in parallel with another capacitor (Figure 3) [53,54,56].

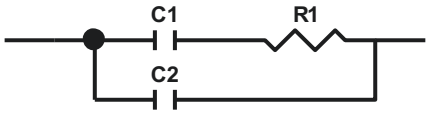

Figure 3. Proposed equivalent circuit to model the dielectric prepared.

The capacitor C_2 accounts for fast dipoles in the material while the capacitor C_1 in series with the resistance R_1 sets the relaxation time for the charge and discharge process $\tau = R_1 \cdot C_1$, and accounts for slow dipoles. At low frequencies ($f << 1/\tau$), the charge-discharge process is slow enough and both capacitors can follow the process so the equivalent capacitance tend to C_1+C_2. However, at high frequencies ($f >> 1/\tau$), the capacitor C_1 is not able to be charged and discharged in every cycle of applied voltage and the equivalent capacitance must tend to C_2.

Therefore, considering this equivalent circuit (Figure 3) the impedance data fitting should allow obtaining C_1, C_2 and R_1 as fitting parameters and consequently ε_{rd}, ε_{re} and the relaxation time, τ [54]:

$$\varepsilon_{rd} = \frac{C_1 + C_2}{\frac{A}{d}} \quad (9)$$

$$\varepsilon_{re} = \frac{C_2}{\frac{A}{d}} \quad (10)$$

$$\tau = R \cdot C_1 \quad (11)$$

Finally, introducing the values of ε_{rd}, ε_{re} and τ in eq. 7, an estimation of the real, $\varepsilon_r'(f)$, and imaginary, $\varepsilon_r''(f)$, parts of the relative permittivity or the dielectric constant, $\varepsilon_r(f)$, as a function of frequency can be achieved.

$$\varepsilon_r{}'(f) = \frac{d}{A\varepsilon_0} \cdot \left[C_2 + \frac{C_1}{1 + (2\pi f)^2\,\tau^2}\right] \quad (12)$$

$$\varepsilon_r{}''(f) = \frac{d}{A\varepsilon_0} \cdot \left[\frac{2\pi f\tau\, C_1}{1 + (2\pi f)^2\,\tau^2}\right] \quad (13)$$

If the equivalent circuit shown in Figure 3 does not satisfy the dielectric behavior of the materials under consideration, the relative permittivity, ε_r, and other electrical parameters of could be estimated using other more known and conventional relations, as for example [55,57]:

$$\varepsilon' = \frac{Z''}{\omega C_0 (Z'^2 + Z''^2)} \quad (14)$$

$$\varepsilon'' = \frac{Z'}{\omega C_0 (Z'^2 + Z''^2)} \quad (15)$$

where $C_0 = \varepsilon_0 A/d$.

Furthermore, both models can provide information about the loss factor parameter:

$$tan\delta(\omega) = \frac{\varepsilon''}{\varepsilon'} \quad (16)$$

where δ is the phase shift.

Piezoelectric characterization of the specimens was carried out taking the electrical response of the materials when a fast load (impact) is applied from the free fall of a stainless steel cylinder of 2 mm of diameter, 10 mm of height and 0.25 g. A photograph of the set-up for the piezoelectric test is shown in Figure 4.

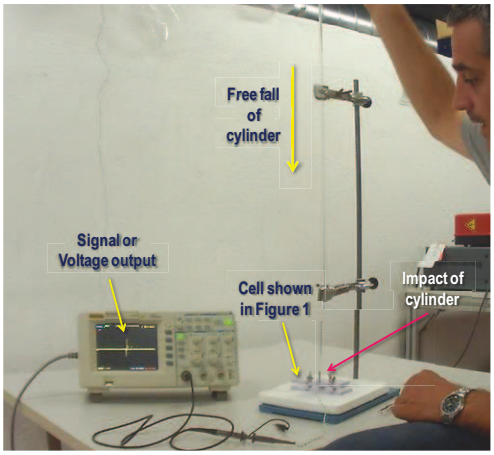

Figure 4. Experimental set-up to measure the output voltage generated from the impact of a free falling cylinder.

RESULTS AND DISCUSSION

As example of particle dispersion, SEM images of some samples in the form of films with high loads of $BaTiO_3$ are shown in Figure 5. Brighter domains in the SEM images obtained from the signal of BES reflect the presence of heavier elements. Images b), c) and d) of Figure 5 show quite well separated bright domains (~ 250 nm of mean diameter), which denote the presence of Ba and Ti. EDAX microanalysis was performed on the bright domains obtaining X-ray spectra in which the presence of Ba and Ti is confirmed (not shown). These results point out how HEBM helps to separate the $BaTiO_3$ particles from the as received agglomerates and embed them within the PVDF matrix, as a prior step to obtain the final films of composites with uniform dispersion of submicrometric particles.

The crystalline structure of all the samples was analyzed from the X-ray diffractograms shown in Figure 6. In every case, the peaks associated to the stable α-phase can be observed, with characteristic reflections at 2θ = 17.9º (100), 18.7º (020), 20.2º (110), and 26.9º (021). At this point it is worth mentioning that some authors claim that the peak at 20.2º belongs to both the α and β phases respectively. In particular, to the (110) reflection of the α-phase and the (200)/(110) reflections of the β-phase [58]. However, it is generally accepted that when β-phase coexists with α-phase the diffraction peak at 20.2º shifts to 19.9º, and a new diffraction peak appears at 20.7º which corresponds to the (200)/(110) reflections of the β-phase [59]. On the other hand, for the samples containing $BaTiO_3$ particles the typical diffraction peaks of its tetrahedral form can be observed [50]. The peak at 17.9º is the only one, among the major alpha characteristic peaks, that does not show overlapping reflections with those of the γ or β phases [60]. Therefore, the simple inspection of a relative decrease in that peak (100) would imply an increase in the content of other phase or phases. It was observed that the relative intensity of the PVDF diffraction peaks (Figure 6) was not affected by the presence of any of the particles ($BaTiO_3$ and MWCNT).

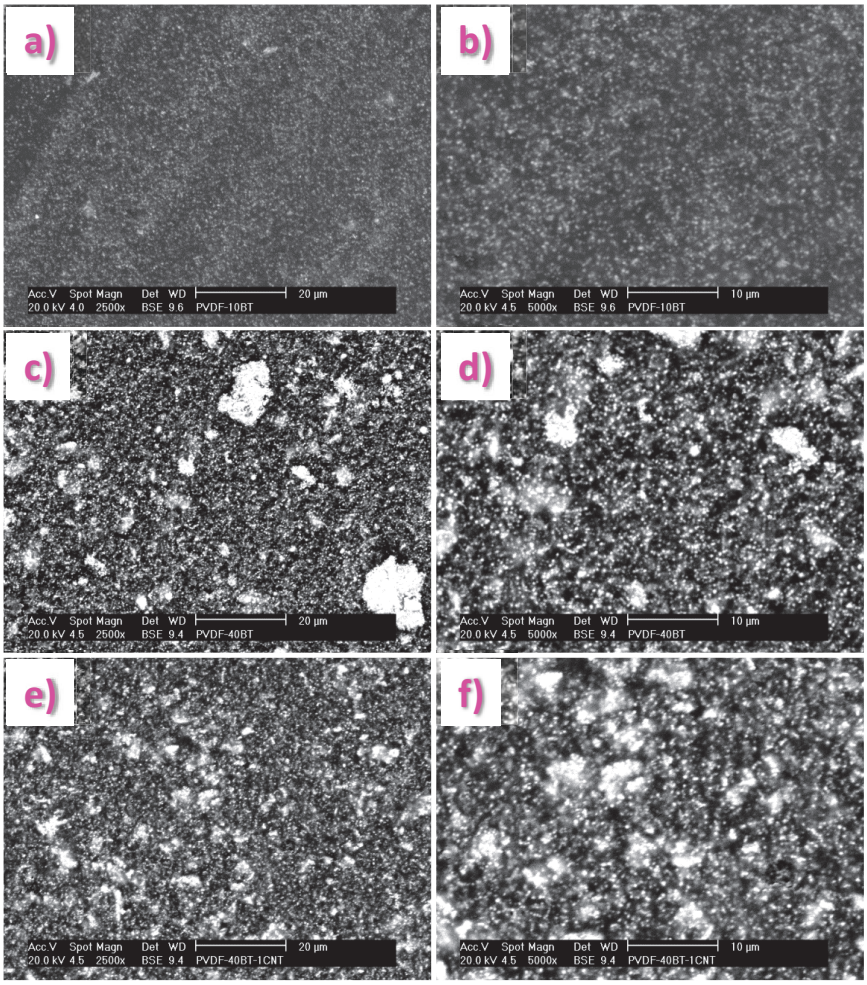

Figure 5.- SEM images of PVDF-based composites obtained from the BSE signal: a) and b) 10% wt of $BaTiO_3$; c) and d) 40% wt of $BaTiO_3$; e) and f) 40% wt of $BaTiO_3$ and 1% wt of MWCNT.

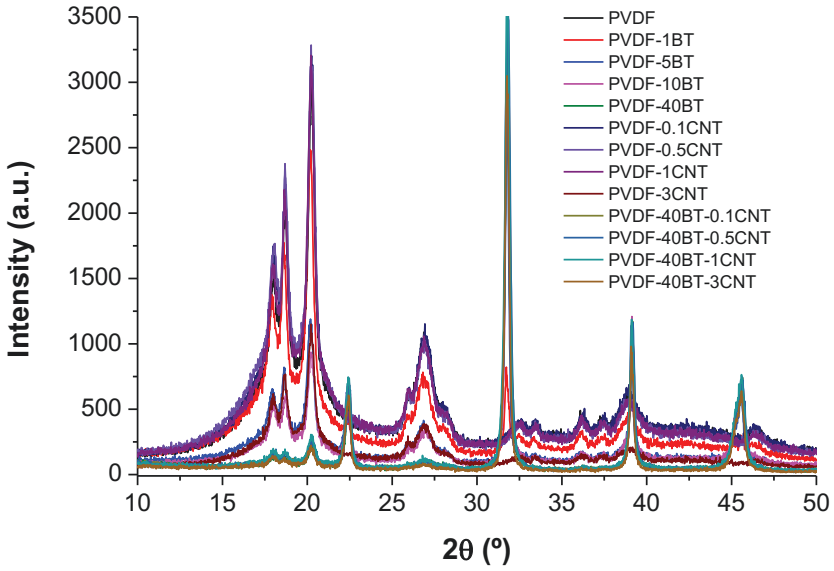

Figure 6.- XRD patterns of the samples under study.

Therefore, it can be said that the addition of BT, MWNT, or a mixture of BT plus MWCNT has not any influence on the PVDF polymorphism, at least for the compositions studied and under the processing conditions used in this work.

However, apparently opposite results were found by other researchers regarding the influence of MWCNT and $BaTiO_3$ on the PVDF structure. They can be summarized as follows: i) the fillers seem to favor the formation β and γ phases and ii) the fillers do not induce any change in the polymorphs contribution. However, although apparently contradictory all the results may be right since there is another variable that has not been taken into account, the final processing method to obtain the material. When the final processing implies hot pressing or melting, in other words, when PVDF crystallizes from the melt but, at low or relatively low temperatures (below 100ºC), the α-phase is mainly obtained [60,61] and many changes are not observed on adding MWCNT or BT [62,63]. However, when solvent casting is used or PVDF crystallization occurs from solution (at least for certain solvent casting rates), large amounts of β and γ phase can be obtained, being even enhanced by the presence of certain nanofillers [18,61,64]. One possible reason may be the proper process of casting (solvent evaporation rate) that can be modified when nanoparticles participate. The competing interactions filler-polymer, polymer-solvent, filler-solvent should influence the solvent evaporation process.

FTIR-ATR spectra of the nanocomposites and neat PVDF films are shown in Figure 7. In order to make better comparisons specific sets of spectra are depicted in Figure 7: a) spectra as a function of $BaTiO_3$ content; b) spectra as a function of MWCNT content; and c) spectra as a function of MWCNT when the amount of $BaTiO_3$ is set at 40 wt%. In each case, the main characteristic absorption bands of the α-phase at 1214, 974, 794 and 764 cm^{-1} are observed. Besides, a small contribution of the γ and β phases are present as small bands at 842 cm^{-1} and 1278 cm^{-1}, which are usually assigned to vibrations appearing in those phases [60,62,65,66]. By using the absorbance at 1072 cm^{-1} as a reference to normalize the FTIR spectra (this band was indentified to be proportional to the film thickness, regardless the crystalline changes in the PVDF) [65,67] it can be demonstrated that the relative amount of the crystalline phases remains constant with the composition of the nanocomposites. Therefore, in accordance with DRX results, the addition of $BaTiO_3$, MWNT, or the mixture of BT plus MWCNT has not any influence on the PVDF polymorphism, at least for the processing conditions and compositions used in this work. The only clear difference observed appears in the range 600 - 700 cm^{-1} because the absorbance coming from $BaTiO_3$. As expected, in that IR region the absorbance increases with the amount of BT.

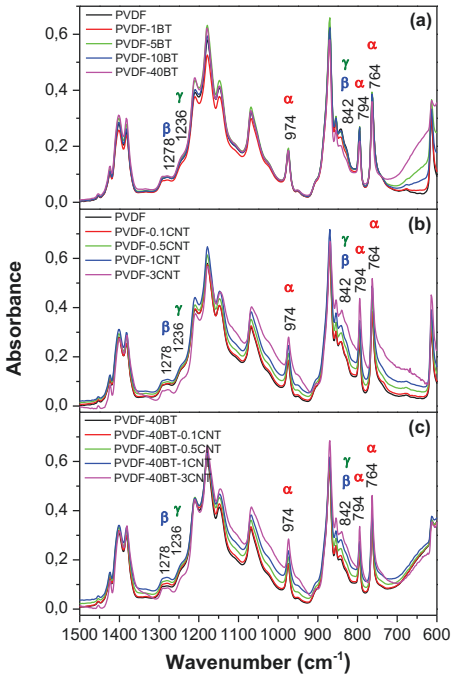

Figure 7. ATR-FTIR spectra of the nanocomposites and neat PVDF films.

Crystallization and melting behavior

The crystallization behavior of PVDF in the ternary nanocomposites was studied using DSC. Figure 8 (left) shows the DSC traces at a 10 °C/min of cooling rate. Although similar exotherm peaks were obtained for all the samples regardless the filler nature and composition, small differences in the width and clear variations in the peak position were observed. The crystallization peak temperatures, T_c, at the exothermic minima and their half widths, HW_c, of all the samples were extracted from the DSC thermograms and gathered in Table 2. There is T_c shift to higher temperatures that can be ascribed to a nucleation effect on the PVDF crystallization due to the presence of $BaTiO_3$ and MWCNT fillers. Besides, the HW_c decreases as the nanoparticles load increases probably due to a narrower distribution of crystallite sizes that, in fact, should be dependent on the nucleation if the crystallization rate increases. Higher induced nucleation causes more starting points of nucleation that, after the corresponding crystal growth, should yield higher homogeneity in terms of structure and morphology, at least if transcrystallinity is not considered.

When MWCNT are used the nucleation effect seems to be enhanced since with the addition of only 3 wt% similar changes in T_c and HW_c were obtained in comparison with the addition of 40 wt% of $BaTiO_3$. This result may be interpreted by considering that changes observed in the PVDF crystallization process are due to the larger surface area of the filler more than to the nature of the nanoparticles. An estimation of the surface per unit of mass for each type of particles can be done using the densities of the materials and assuming that $BaTiO_3$ particles are perfect spheres and MWCNT are perfect cylinders. The results yields a surface area for the MWCNT of about two orders of magnitude higher than for the $BaTiO_3$ particles, which reinforces the above mentioned. Finally, when ternary composites are considered, there exists

a combined effect between $BaTiO_3$ and MWCNT that doubles the shift of the crystallization peak, as expected in terms of the increment in nanofiller surface.

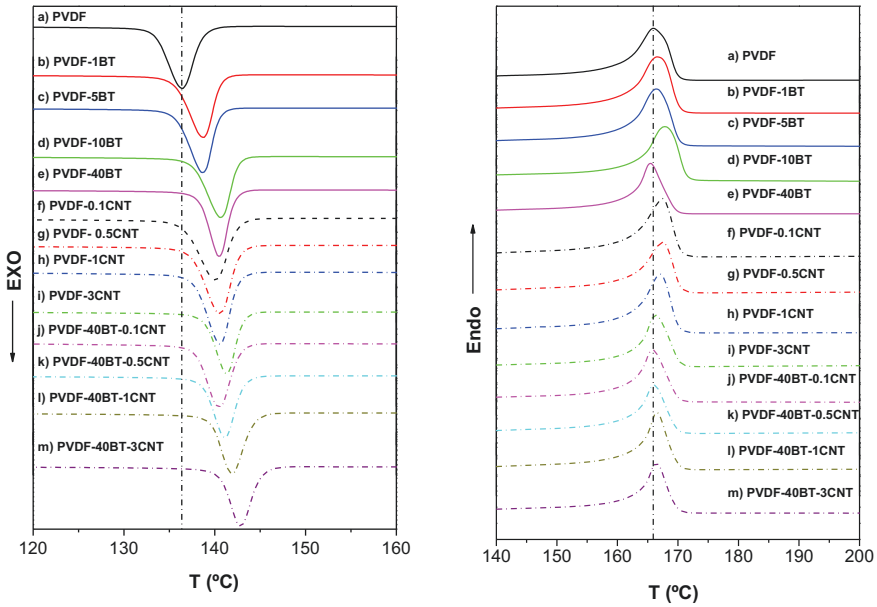

Figure 8. DSC traces obtained by cooling (left) and heating (right) scans.

Table 2. Thermal parameters extracted from the thermograms obtained by the DSC heating and cooling scans (Figure 8).

Sample	First heating T_m (ºC)	Second Heating T_m (ºC)	HW_m (ºC)	T_c (ºC)	HW_c (ºC)	χ (%)
PVDF	167.5	166.0	5.94	136.5	3.53	44.4
PVDF-1BT	167.9	166.5	5.94	138.7	3.32	44.3
PVDF-5BT	168.0	166.5	5.73	138.7	3.12	43.2
PVDF-10BT	169.0	167.8	5.50	140.7	3.26	46.9
PVDF-40BT	167.6	165.5	4.30	140.4	2.45	41.3
PVDF-0.1CNT	168.3	167.4	5.32	140.0	3.88	43.7
PVDF-0.5CNT	168.0	167.5	5.13	140.6	3.44	45.1
PVDF-1.0CNT	168.1	167.1	4.92	140.5	3.17	45.9
PVDF-3.0CNT	169.0	166.3	4.50	141.4	2.82	42.5
PVDF-40BT-0.1CNT	168.0	165.8	4.91	140.4	3.47	43.7
PVDF-40BT-0.5CNT	168.1	166.1	4.91	141.1	3.05	43.9
PVDF-40BT-1.0CNT	168.8	166.5	4.10	142.0	3.16	44.8
PVDF-40BT-3.0CNT	169.4	166.3	4.10	142.8	3.09	44.9

Melting behavior of PVDF in the ternary nanocomposites is shown in the DSC traces of the Figure 8. Regardless the filler nature and composition similar endotherm peaks can be observed with small differences in the peaks position. The melting peak temperatures, T_m, and their half widths, HW_m, extracted from the DSC thermograms, are collected in Table 2. As in the crystallization process, HW_m of the endothermic process decreases as the nanoparticles load increases. This result also suggests, as expected from the previous crystallization processes, a narrow distribution of crystallite sizes.

Finally, the crystallization degree, χ_c, has been obtained from equation 1. Changes lower than 15% in the degree of crystallinity as a function of composition were observed (Table 2). In particular, when the $BaTiO_3$ content increased, χ_c decreased. Likewise, when MWCNT content increased up to 1 wt% χ_c increased, while for a 3% of MWCNT there was a clear decrease in χ_c, being even lower than the crystalline fraction of the neat PVDF. Finally, for a constant amount of 40 w% $BaTiO_3$ there was a very slight increase of χ_c as the amount of MWCNT increased (even for 3 w% of MWCNT). As a conclusion, although some changes can occur in terms of morphology, there were not important variations in the degree of crystallinity as a function of composition for the nanocomposites under study.

Electrical behavior

The capacities measured with the multimeter together with the calculated dielectric constants, ε_r (eq. 2), are shown in Table 3. It is observed how as the $BaTiO_3$ content increases the ε_r value increases, being the increment of 66% when 40 wt% of $BaTiO_3$ (about 18.9 % in fraction volume) was added to the PVDF. In a similar system based on PVDF filled with $BaTiO_3$ Yu et al. found that for a composition of 20% by volume of $BaTiO_3$ there was an increase of the dielectric constant of about 100% respect to that of the neat PVDF [34] what would be in accordance with the results of the present work. The slightly higher increase of ε found by Yu et al can be explained considering that in their research $BaTiO_3$ particles of smaller size were used. As shown elsewhere [4] based on the results of a composite of polystyrene filled with $BaTiO_3$ nanoparticles and where the Effective Medium Theory (EMT) was used [68], a slight enhancement of the dielectric constant is expected in the composite with larger interphase region or smaller the particles size [4]. Besides, the Maxwell-Garnett approximation [69,70] predicts an increase in the dielectric constant of the polymer of about 69% for a composition of 18.9 % by volume of particles, which is very close to that experimentally obtained in this work. The Maxwell-Garnett approximation is reasonable for matrix-based composites consisting of a continuum matrix with embedded inclusions, therefore a suitable model to describe the PVDF/$BaTiO_3$ nanocomposites obtained by HEBM and subsequent hot pressing.

On the other hand, when adding MWCNT to the PVDF matrix there was a greater increase in the relative permittivity as a function of the filler content, around 46% for only 1 wt% of MWCNT. For 3 wt% of MWCNT much sharper increase was observed, almost three orders of magnitude, indicating that a transition in terms of composition occurred. This transition can correspond to that of the percolation threshold. In fact, the percolation threshold for PVDF/MWCNT systems is in the range 1 to 3 weight percent attending to results provided by other authors. For example, the percolation threshold in electrospun PVDF/MWCNT ultrafine

fibers was reported to be 1.2 wt% [71]. Li et al reported a percolation threshold of CNT/PVDF nanocomposites at concentrations of about 2.1 vol% or 2.5 wt% [72]. On the other hand, Lan Wang and Zhi-Min Dang reported a percolation threshold of MWCNT/PVDF nanocomposite of 1.61 vol% or 1.9 wt% [73], while Hong and Hwang [64], who prepared PVDF/multi-walled carbon nanotube (MWCNT) composite films by melt mixing obtained a percolation threshold for the electrical conductivity between 2 wt.% and 2.5 wt.% of MWNT loading.

Table 3. Values of the electrical capacities and corresponding estimated relative permitivities for the different PVDF based nanocomposites.

Samples	Capacity (pF)	Thickness (μm)	ε_r
PVDF	38.0 ± 0.5	107	5.9 ± 0.1
PVDF-1BT	48.0 ± 0.3	107	7.4 ± 0.1
PVDF-5BT	47.8 ± 0.8	108	7.4 ± 0.1
PVDF-10BT	50.0 ± 0.3	111	8.0 ± 0.1
PVDF-40BT	60.0 ± 0.6	113	9.8 ± 0.1
PVDF-0.1CNT	43.0 ± 0.3	108	6.7 ± 0.1
PVDF-0.5CNT	45.0 ± 0.4	114	7.4 ± 0.1
PVDF-1CNT	57.0 ± 0.1	105	8.6 ± 0.1
PVDF-3CNT	749 ± 1.0	108	116.3 ± 0.2
PVDF-40BT-0.1CNT	66.0 ± 0.3	113	10.7 ± 0.1
PVDF-40BT-0.5CNT	69.0 ± 0.6	106	10.5 ± 0.1
PVDF-40BT-1CNT	80.0 ± 0.8	110	12.7 ± 0.1
PVDF-40BT-3CNT	777 ± 32	108	120.7 ± 5.0

The most remarkable data relative to the dielectric behavior of the nanocomposites as a function of the frequency are collected in Table 4. In all cases the equivalent circuit represented in Figure 1 has been used to model the dielectric behavior and the corresponding equations to fit the data of impedance. The system containing 3% of MWCNT, as an exception, was not able to be described by model of figure 1 because, as expected, the material must cease to behave completely as a dielectric once the percolation threshold has been overcome.

As an example, the real and imaginary parts of the relative permittivity and the loss tangent obtained from impedance data were plotted as a function of frequency for the sample PVDF-1BT (Figure 9). For comparison, data obtained from the two theoretical approaches or methods considered in the experimental part were also shown (Figure 9): a) using the RC equivalent model (eqs. 10 and 11); and b) using eqs. 12 and 13.

Table 4. Relative permittivities, ε', at three frequencies: the frequency of the dipole relaxation, f_m, 1 kHz (f_{1kHz}) and 1 MHz (f_{1MHz}) and calculated and experimental relaxation times, τ and $1/f_m$, respectively.

Sample	ε' (at f_m)	ε' (at f_{1KHz})	ε' (at f_{1MHz})	τ ×10^2 (s)	($1/f_m$) ×10^2 (s)
PVDF	16.7 ± 3.3 (13.9 ± 3.5)	8.7 ± 1.5 (8.5 ± 1.4)	8.7 ± 1.5 (9.2 ± 0.4)	7.7 ± 0.1	3.55 (3.16)
PVDF-1BT	18.5 ± 0.9 (15.1 ± 2.5)	9.5 ± 0.8 (9.3 ± 1.1)	9.8 ± 0.8 (8.8 ± 1.0)	7.7 ± 0.1	3.98 (3.55)
PVDF-5BT	17.9 ± 3.2 (14.9 ± 2.0)	9.0 ± 2.0 (9.0 ± 1.3)	9.0 ± 2.0 (9.1 ± 1.1)	7.7± 0.1	3.98 (3.55)
PVDF-10BT	21.0 ± 2.0 (18.5 ± 0.5)	10.6 ± 1.0 (10.1 ± 0.2)	10.6 ± 1.0 (9.5 ± 0.2)	7.7 ± 0.1	3.98 (3.98)
PVDF-40BT	24.2 ± 2.6 (18.2 ± 2.0)	12.0 ± 1.0 (11.4 ± 0.6)	12.0 ± 1.0 (11.1 ± 0.5)	7.7± 0.1	4.47 (3.98)
PVDF-0.1CNT	23.2 ± 2.2 (20.6 ± 1.0)	10.9 ± 1.0 (11.0 ± 0.4)	10.9 ± 1.0 (9.9 ± 0.6)	7.6 ± 0.1	3.98 (4.47)
PVDF-0.5CNT	23.8 ± 1.4 (21.9 ± 2.0)	12.0 ± 0.4 (11.9 ± 0.5)	12.0 ± 0.4 (11.3 ± 1.1)	7.6 ±0.1	4.47 (3.98)
PVDF-1.0CNT	25.0 ± 1.3 (22.4 ± 1.4)	12.4 ± 1.0 (12.5 ± 0.3)	12.4 ± 1.0 (11.7 ± 1.1)	7.6± 0.1	4.47 (4.47)
PVDF-3.0CNT	51.2 ± 6.3 (123 ± 24)	24.9 ± 3.3 (43.0 ± 3.0)	24.9 ± 3.3 (22.0 ± 4.0)	-	- (6.61)
PVDF-40BT-0.1CNT	29.8 ± 1.0 (23.0 ± 4.0)	14.7 ± 0.2 (13.0 ± 1.0)	14.7 ± 0.2 (13.1 ± 1.0)	7.6 ± 0.1	5.01 (5.01)
PVDF-40BT-0.5CNT	27.9 ± 4.2 (24.1 ± 4.1)	13.8 ± 1.3 (13.4 ± 0.3)	13.8 ± 1.3 (11.8 ± 0.8)	7.657 ± 0.1	
PVDF-40BT-1.0CNT	32.9 ± 2.6 (33.9 ± 4.3)	17.4 ± 1.0 (17.8 ± 1.1)	17.4 ± 1.0 (15.6 ± 0.5)	7.5 ± 0.1	
PVDF-40BT-3.0CNT	97.0 ± 12.2 (110 ± 34)	49.3 ± 7.2 (68.8 ± 7.8)	49.3 ±7.2 (30.5 ± 3.5)	-	

As can be observed, both methods provide similar results except in the low frequency region for which the method a) showed higher values of the real part of the relative permittivity. At low frequencies ($f << 1/\tau$), the charge-discharge process is slow enough for both capacitors to be charged and the equivalent capacity should tend to one capacitance of value C1+C2 (with the exception of materials with 3 wt% of MWCNT, where almost a resistive behavior is shown). However, at high frequencies ($f >> 1/\tau$), the capacitor C1 is not able to be charged and discharged in every cycle of applied voltage so the equivalent capacitance tends to C2. At frequencies close to $1/\tau$, some dipoles are able to rotate completely, but with great friction among them, leading to a more resistive behavior.

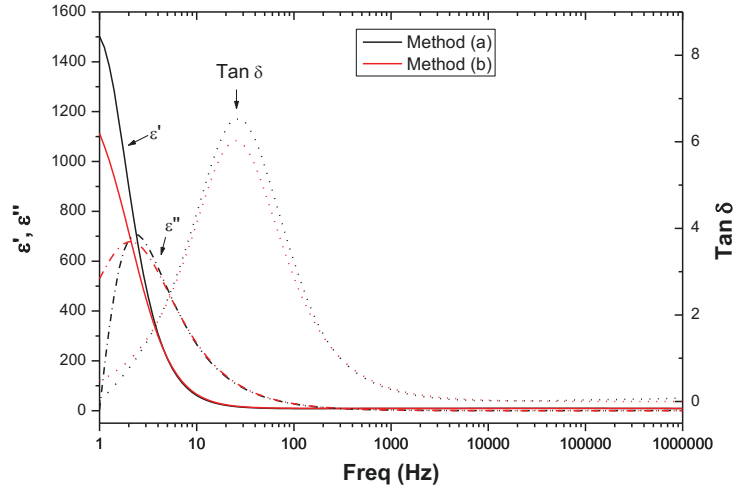

Figure 9. Real (continuous lines) and imaginary (dashed lines) parts of the relative permittivity, and the loss tangent (dot lines) obtained from impedance data as a function of frequency (sample PVDF-1BT).

The relative permittivities at different frequencies: a) the frequency of the dipole relaxation, f_m (maximum of the loss factor, Tan δ); b) 1 kHz, f_{1kHz}, and c) 1 MHz, f_{1MHz}, are gathered in Table 4, together with the relaxation time of C1, τ, and the relaxation time experimentally obtained from the frequency at the maxima of the loss factor, $1/f_m$. Taking into account the similarity between the values of τ and $1/f_m$ one would expect that the relaxation given by the maxima of the loss factor was due to relaxation of the charge-discharge process associated to the orientation of slower dipoles.

As can be seen, the relative permittivities in Table 4 are different from those presented in Table 3 since the measurement method is completely different. In the first case (Table 3) the capacitance of the samples was measured when the steady state is reached from a constant applied voltage; thus, it only takes into account the slower polarization mechanisms.

In Figures 10a and b the frequency responses of the real part of the permittivity and the loss tangent (dielectric loss) are illustrated, respectively.

As can be seen the dielectric constant of the nanocomposites increased in comparison to the neat PVDF polymer over the entire range of frequencies (from 1 Hz to 1 $\times 10^6$ Hz) (Figure 10 and Table 4). Besides, regardless the frequency, the higher amount of particles the higher the relative permittivity of the composite. On the other hand, the effect induced by the MWCNT is more important, being even sharper for 3% wt of MWCNT. When comparing the materials with 40% wt of $BaTiO_3$ it is also observed a further increase of permittivity with the addition of MWCNT. This result might be due to the fact that the concentration of $BaTiO_3$ and MWCNT influences the resultant polarization in the composites system as it happened in other PVDF filled composites [31]. One possible explanation can be the interfacial polarization that should

tend to infinite above the percolation threshold when conductive particles are used as the filler. Interfacial polarization is widely observed in heterogeneous systems with phases having different conductivities or dielectric permittivities, such as conductive polymer composites, CPCs [74,75]. It takes place because of the accumulation of mobile charges at the interface of unlike phases with different electrical conductivities or permittivities. As interfacial polarization occurs at large scale (mesoscopic scale), it has usually been observed at low frequencies, due to its large relaxation time with respect to the frequency of the electric field [74].

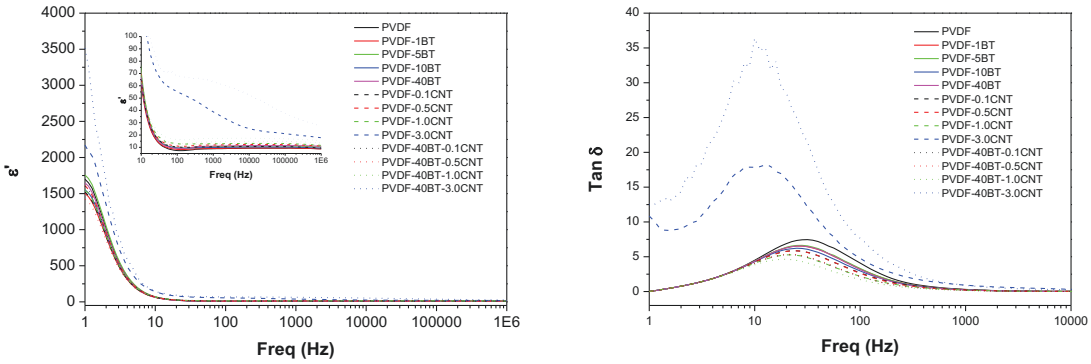

Figure 10. Frequency responses of the dielectric constant (a) and loss tangent (b) for all the materials under study.

Other explanation for the results shown in Table 4 can be based on changes in the crystallinity degree. An enhancement of the crystallinity may cause molecules aligning in a much ordered conformation with better molecular chain packing, which in turn would increase the dipole density in the system and would lead to an increase in the dielectric constant. However, the crystallinity degree of PVDF in the samples is almost the same regardless the composition. Therefore, this cannot be the cause of the different dielectric behaviors observed.

It was also observed that the permittivity of all the materials under study exhibited strong frequency dependence. In general, the permittivity quickly decreased in the low-frequency range (up to 100 Hz), and slightly increased in the high frequency range (see inset of Figure 10a). There was an exception for the materials with a 3% wt of MWCNT since, in the entire frequency range, they shown a continuous decrease in the dielectric constant very moderate from 100 Hz. This behavior is usually ascribed to the large delay of the interfacial polarization respect to the electric field oscillation at high frequencies (relaxation phenomenon) [7,76]. In fact, at high enough frequencies, the electric field oscillation may be too fast as to impede the free electrons to pile up at the interface. However, in the insulate region, due to the lack of interfacial polarization, the dielectric permittivity is independent of frequency.

On the other hand, it is observed how, in general terms, there is a decrease in the loss factor when $BaTiO_3$ and MWCNT are in the PVDF matrix, being the effect enhanced when increasing the concentration of particles (see figure 10b). Besides, the effect of MWCNT is more

important since only the addition of 0.1% of MWCNT (sample PVDF-0.1CNT) reduces the loss factor by 10% respect to the composite with 40% of $BaTiO_3$ (sample PVDF-40BT). When both types of fillers are present, an additive effect was observed, only if the amount of MWCNT is high enough the opposite effect was observed, the dielectric losses greatly increased for the composite with 3% wt of MWCNT. In principle, an increase in the loss factor was expected at any concentration of fillers, at least when they are conductive because of electrical leaking; however, below the percolation threshold (3% wt of MWCNT) the opposite effect was observed. Previous reports [34] provided an explanation to this apparent contradictory behavior. The incorporation of nanoparticles can decrease the crystalline size of the PVDF polymer, leading to the reduction of the dielectric loss due to the reversal of dipoles up to a certain percolation limit [77]. However, in this work structural evidences about changes in the crystalline size of PVDF were not found (changes in the XRD half peak width, for instance), pointing out to a different reason. One possible explanation may be the influence of the filler on the dynamics of the polymer, hindering the motion of the charge carriers. In fact, the relaxation phenomenon ascribed to the slower dipole and represented by the maxima of the loss factor shifts to lower frequencies when nanoparticles are within the PVDF. In this case, the effect of MWCNT was also more important. This result can be explained if the restriction to the polymer motion is due to direct interaction between polymer chains and filler surface. It is clear that MWCNT present a quite higher surface to volume ratio than $BaTiO_3$ particles so more influence on the PVDF dynamics is expected for the MWCNT.

Finally, the increase of dielectric loss with conductive filler content can be attributed to enhanced Ohmic and polarization losses. At high MWCNT contents (over the percolation threshold), the amount of dissipating nomadic charges is higher. Moreover, an increase in filler content leads to the formation of a conductive network (percolation threshold) in which the electrons have greater free paths to move in each half cycle of alternating field, thereby dissipating more electrical energy [78,79]. All these phenomena lead to higher Ohmic loss, which is linked to dissipation of energy in phase with the alternating field (specially, for lower frequencies). In addition, the augmented polarization loss arising from interfacial polarization is another significant factor increasing the dielectric loss at higher MWCNT contents.

Finally, Figure 11 shows the piezoelectric results from three tests on one specimen of neat PVDF and the mean values of the output voltage as a function of the type of material.

As can be seen, within the experimental uncertainty, the output voltage after the impact is similar regardless the composition of the composites (Figure 11 right). Therefore, it can be concluded that the piezoelectric behavior does not seem to be affected by the incorporation of the nanofillers, at least, for the compositions under study. Again, the MWCNT 3% wt is the exception since there is a clear decrease in the output voltage signal extracted from the oscilloscope. A possible explanation to this is the high dielectric loss (see figure 10b) experienced by a material which has become conductive above the percolation threshold. Therefore, the combination of $BaTiO_3$ particles with small amount of MWCNT, below the percolation threshold, can highly increase the relative permittivity of PVDF and decrease the dielectric losses without compromising other properties as its piezoelectric performance.

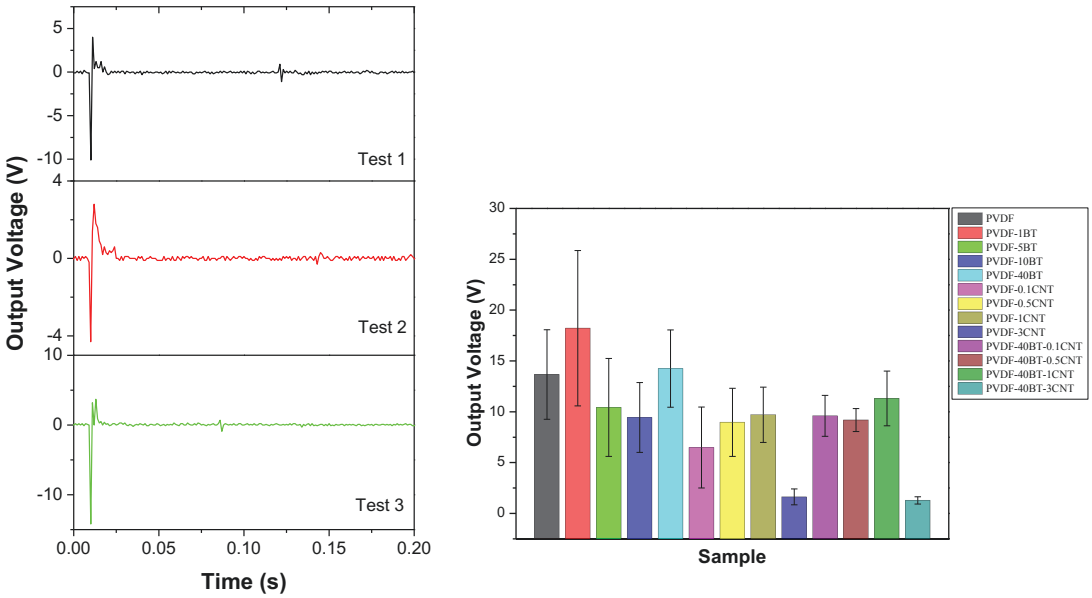

Figure 11. Piezoelectric results for three tests on one specimen of the neat PVDF (left) and mean output voltages for all materials (right).

CONCLUSION

PVDF/$BaTiO_3$/MWCNT ternary nanocomposites in the form of films were prepared by a mixing process of high energy ball milling, HEBM, and subsequent hot pressing. It has been demonstrated that HEBM helps to separate the $BaTiO_3$ nanoparticles from the as received agglomerates and embed them in the PVDF matrix to finally obtain films of composites with uniform dispersion of the submicrometric particles.

The addition of $BaTiO_3$ and MWCNT had not any influence on the PVDF polymorph and very little on the melting and crystallization from the melt, at least for the compositions studied and under the processing conditions used in this work. The main changes observed were associated to the presence of MWCNT and seems to be a consequence of more available filler surface.

The capacitance of the composites increased as the nanofiller contain increased, being the effect mainly dependent again on the surface to volume ratio of the nanoparticles. The dielectric behavior of the materials as a function of frequency was possible to be modeled by a Debye equivalent circuit only below the MWCNT percolation threshold. This phenomenon was attributed to the interfacial polarization that should tend to infinite over the percolation threshold when conductive particles are used as the filler.

Finally, the analysis of the piezoelectric characteristics of the materials allowed concluding that the combination of $BaTiO_3$ with small concentrations of MWCNT (below percolation threshold), leads to remarkable increases of permittivity and reductions in dielectric losses of PVDF without compromising its piezoelectric properties.

ACKNOWLEDGMENTS

Authors gratefully acknowledge financial support from the Ministerio de Ciencia e Innovación (MAT2010-16815) and the Ministerio de Asuntos Exteriores y de Cooperación and the Agencia Española de Cooperación Internacional para el Desarrollo for supporting the PhD Thesis of Freddy Ariel Sanchez.

REFERENCES

1. Gregorio, R.; Cestari, M.; Bernardino, F. E. *J. Mater. Sci.* **1996**, *31*, 2925.
2. Bai, Y.; Cheng, Z.-Y.; Bharti, V.; Xu, H. S.; Zhang, Q. M. *Appl. Phys. Lett.* **2000**, *76*, 3804.
3. Olmos, D.; Martínez-Tarifa, J. M.; González-Gaitano, G.; González-Benito, J. *Polym. Test.* **2012**, *31*, 1121.
4. Dang, Z. M.; Shen, Y.; Nan, C. W. *Appl. Phys. Lett.* **2003**, *81*, 4814.
5. Dang, Z. M.; Fan, L. Z.; Shen, Y.; Nan, C. W. *Chem. Phys. Lett.* **2003**, *369*, 95.
6. Yao, S.-H.; Dang, Z.-M.; Jiang, M.-J.; Bai, J. *Appl. Phys. Lett.* **2008**, *93*, 182905.
7. Dang, Z. M.; Yuan, J. K.; Zha, J. W.; Zhou, T.; Li, S. T.; Hu, G. H. Fundamentals, processes and applications of high-permittivity polymer-matrix composites. *Prog. Mater. Sci.* **2012**, *57*, 660–723.
8. Choi, H. W.; Heo, Y. W.; Lee, J. H.; Kim, J. J.; Lee, H. Y.; Park, E. T.; Chung, Y. K. *Appl. Phys. Lett.* **2006**, *89*.
9. Zhou, Y.; Bai, Y.; Yu, K.; Kang, Y.; Wang, H. *Appl. Phys. Lett.* **2013**, *102*, 252903.
10. Da Silva, A. B.; Arjmand, M.; Sundararaj, U.; Bretas, R. E. S. *Polym. (United Kingdom)* **2014**, *55*, 226.
11. Pecharromán, C.; Moya, J. S. *Adv. Mater.* **2000**, *12*, 294.
12. Dang, Z. M.; Yao, S. H.; Yuan, J. K.; Bai, J. *J. Phys. Chem. C* **2010**, *114*, 13204.
13. Olmos, D.; Domínguez, C.; Castrillo, P. D.; Gonzalez-Benito, J. *Polymer (Guildf).* **2009**, *50*, 1732.
14. Olmos, D.; Montero, F.; González-Gaitano, G.; González-Benito, J. Structure and morphology of composites based on polyvinylidene fluoride filled with BaTiO3 submicrometer particles: Effect of processing and filler content. *Polym. Compos.* **2013**, *34*, 2094–2104.
15. Sánchez, F. a.; Redondo, M.; González-Benito, J. *J. Appl. Polym. Sci.* **2015**, *132*, 41497 (1.
16. Chen, E.-C.; Wu, T.-M. *Polym. Degrad. Stab.* **2007**, *92*, 1009.
17. Feng, J.; Sui, J.; Cai, W.; Wan, J.; Chakoli, A. N.; Gao, Z. *Mater. Sci. Eng. B Solid-State Mater. Adv. Technol.* **2008**, *150*, 208.
18. Yue, X. U.; Wei-tao, Z.; Wen-xue, Y. U.; Li-gui, H. U. a; Yu-jie, Z.; Zhu-di, Z. *Chem. Res. Chinese Univ.* **2009**, *26*, 491.
19. Chen, Q. X.; Payne, P. a *Meas. Sci. Technol.* **1995**, *6*, 249.
20. Gregorio, R.; Capitão, R. C. *J. Mater. Sci.* **2000**, *35*, 299.
21. Gregorio, R.; Borges, D. S. *Polymer (Guildf).* **2008**, *49*, 4009.
22. Nunes, J. S.; Wu, A.; Gomes, J.; Sencadas, V.; Vilarinho, P. M.; Lanceros-Mendez, S. *Appl. Phys. a-Materials Sci. Process.* **2009**, *95*, 875.
23. Gomes, J.; Serrado Nunes, J.; Sencadas, V.; Lanceros-Mendez, S. *Smart Mater. Struct.* **2010**, *19*, 065010.

24. Grossman, E.; Gouzman, I. In *Nuclear Instruments and Methods in Physics Research, Section B: Beam Interactions with Materials and Atoms*; **2003**; Vol. 208, pp 48.
25. Gonzalez, R. I.; Phillips, S. H.; Hoflund, G. B. *J. Appl. Polym. Sci.* **2004**, *92*, 1977.
26. Fang, F.; Yang, W.; Zhang, M. Z.; Wang, Z. *Compos. Sci. Technol.* **2009**, *69*, 602.
27. Ploss, B.; Ploss, B.; Shin, F. G.; Chan, H. L. W.; Choy, C. L. *Appl. Phys. Lett.* **2000**, *76*, 2776.
28. Ploss, B.; Ploss, B.; Shin, F. G.; Chan, H. L. W.; Choy, C. L. *IEEE Trans. Dielectr. Electr. Insul.* **2000**, *7*, 517.
29. Furukawa, T.; Ishida, K.; Fukada, E. *J. Appl. Phys.* **1979**, *50*, 4904.
30. Ploss, B.; Ng, W. Y.; Chan, H. L. W.; Ploss, B.; Choy, C. L. *Compos. Sci. Technol.* **2001**, *61*, 957.
31. Fan, B.-H.; Zha, J.-W.; Wang, D.; Zhao, J.; Dang, Z.-M. *Appl. Phys. Lett.* **2012**, *100*, 12903.
32. Satapathy, S.; Gupta, P. K.; Varma, K. B. R. *J. Phys. D. Appl. Phys.* **2009**, *42*, 055402.
33. Yu, K.; Niu, Y.; Bai, Y.; Zhou, Y.; Wang, H. *Appl. Phys. Lett.* **2013**, *102*, 102903.
34. Yu, K.; Wang, H.; Zhou, Y.; Bai, Y.; Niu, Y. **2013**, *034105*, 3.
35. Zhou, T.; Zha, J. W.; Cui, R. Y.; Fan, B. H.; Yuan, J. K.; Dang, Z. M. *ACS Appl. Mater. Interfaces* **2011**, *3*, 2184.
36. Zha, J.-W.; Dang, Z.-M.; Yang, T.; Zhou, T.; Song, H.-T.; Li, S.-T. *IEEE Trans. Dielectr. Electr. Insul.* **2012**, *19*, 1312.
37. Lopes, A. C.; Carabineiro, S. A. C.; Pereira, M. F. R.; Botelho, G.; Lanceros-Mendez, S. *ChemPhysChem* **2013**, *14*, 1926.
38. Park, H. H.; Choi, Y.; Park, D. J.; Cho, S. Y.; Yun, Y. S.; Jin, H. J. *Fibers Polym.* **2013**, *14*, 1521.
39. He, F.; Fan, J.; Lau, S. *Polym. Test.* **2008**, *27*, 964.
40. Zhang, Y.; Jiang, S.; Fan, M.; Zeng, Y.; Yu, Y.; He, J. *J. Mater. Sci. Mater. Electron.* **2013**, *24*, 927.
41. Linghao He, Qun Xu, Chengwu Hua, R. S. *Polym. Compos.* **2010**, *16*, 921.
42. Linghao He, Jing Sun, Xiaoli Zheng, Qun Xu, R. S. *Polym. Polym. Compos.* **2010**, *21*, 449.
43. He, L.; Zheng, X.; Xu, Q. *J. Phys. Chem. B* **2010**, *114*, 5257.
44. Kim, P.; Jones, S. C.; Hotchkiss, P. J.; Haddock, J. N.; Kippelen, B.; Marder, S. R.; Perry, J. W. *Adv. Mater.* **2007**, *19*, 1001.
45. Yang, M.; Dan, Y. *Colloid Polym. Sci.* **2005**, *284*, 243.
46. Ash, B. J.; Siegel, R. W.; Schadler, L. S. *Macromolecules* **2004**, *37*, 1358.
47. Bikiaris, D. N.; Vassiliou, A.; Pavlidou, E.; Karayannidis, G. P. *Eur. Polym. J.* **2005**, *41*, 1965.
48. Reynaud, E.; Jouen, T.; Gauthier, C.; Vigier, G.; Varlet, J. *Polymer (Guildf).* **2001**, *42*, 8759.
49. Castrillo, P. D.; Olmos, D.; Amador, D. R.; González-Benito, J. *J. Colloid Interface Sci.* **2007**, *308*, 318.
50. Serra-Gómez, R.; González-Gaitano, G.; González-Benito, J. *Polym. Compos.* **2012**, *33*, 1549.
51. Olmos, D.; Rodríguez-Gutiérrez, E.; González-Benito, J. *Polym. Compos.* **2012**, *33*, 2009.
52. Rosenberg, Y.; Siegmann, A.; Narkis, M.; Shkolnik, S. *J. Appl. Polym. Sci.* **1991**, *43*, 535.
53. Scaife, B. K. P. *Principles of Dielectrics*; Oxford University Press, **1998**.
54. Hippel, A. R. Von *Dielectric materials and applications : papers by twenty-two*

contributors; Hippel, A. R. Von, Ed.; Cambridge: M.I.T. Press: New York, **1966**.
55. Tripathi, S. K.; Gupta, A.; Kumari, M. *Bull. Mater. Sci.* **2012**, *35*, 969.
56. Jonscher, A. K. *J. Phys. D. Appl. Phys.* **1999**, *32*, R57.
57. McCrum, N.; Williams, B.; Read, G. *Polymer (Guildf).* **1968**, *9*, 559.
58. Liu, Y. L.; Li, Y.; Xu, J. T.; Fan, Z. Q. *ACS Appl. Mater. Interfaces* **2010**, *2*, 1759.
59. Martins, P.; Costa, C. M.; Botelho, G.; Lanceros-Mendez, S.; Barandiaran, J. M.; Gutierrez, J. *Mater. Chem. Phys.* **2012**, *131*, 698.
60. Ince-Gunduz, B. S.; Alpern, R.; Amare, D.; Crawford, J.; Dolan, B.; Jones, S.; Kobylarz, R.; Reveley, M.; Cebe, P. *Polymer (Guildf).* **2010**, *51*, 1485.
61. Tang, X. G.; Hou, M.; Zou, J.; Truss, R.; Yang, M.; Zhu, Z. *Compos. Sci. Technol.* **2012**, *72*, 263.
62. Ramasundaram, S.; Yoon, S.; Kim, K. J.; Park, C. *J. Polym. Sci. Part B Polym. Phys.* **2008**, *46*, 2173.
63. Chiu, F. C. *Mater. Chem. Phys.* **2014**, *143*, 681.
64. Hong, S. M.; Hwang, S. S. *J. Nanosci. Nanotechnol.* **2008**, *8*, 4860.
65. Benz, M.; Euler, W. B. *J. Appl. Polym. Sci.* **2003**, *89*, 1093.
66. Mandal, D.; Henkel, K.; Schmeisser, D. *J. Phys. Chem. B* **2011**, *115*, 10567.
67. Mandal, A.; Nandi, A. K. *ACS Appl. Mater. Interfaces* **2013**, *5*, 747.
68. Wong, C. P.; Marinis, T.; Jianmin Qu; Yang Rao *IEEE Trans. Components Packag. Technol.* **2000**, *23*, 680.
69. Nan, C.-W. *Prog. Mater. Sci.* **1993**, *37*, 1.
70. Nan, C.-W. *Phys. Rev. B* **2001**, *63*, 176201.
71. Wang, S.-H.; Wan, Y.; Sun, B.; Liu, L.-Z.; Xu, W. *Nanoscale Res. Lett.* **2014**, *9*, 1.
72. Li, L.; Zhang, M.; Ruan, W. *Polym. Compos.* **2015**, *36*, 2248.
73. Wang, L.; Dang, Z.-M. *Appl. Phys. Lett.* **2005**, *87*, 042903.
74. Dakin, T. W. *IEEE Electr. Insul. Mag.* **2006**, *22*, 11.
75. Cruz-Estrada, R. H.; Folkes, M. J. *J. Mater. Sci. Lett.* **2002**, *21*, 1427.
76. Jiang, M. J.; Dang, Z. M.; Bozlar, M.; Miomandre, F.; Bai, J. *J. Appl. Phys.* **2009**, *106*.
77. Elzayat, M. Y. F.; El-Sayed, S.; Osman, H. M.; Amin, M. *Polym. Eng. Sci.* **2012**, *52*, 1945.
78. Arjmand, M.; Apperley, T.; Okoniewski, M.; Sundararaj, U. *Carbon N. Y.* **2012**, *50*, 5126.
79. Steeman, P.; Turnhout, J. *Dielectric properties of inhomogeneous media in: "Broadband dielectric spectroscopy";* Kremer, F.; Schönhals, A., Eds.; Springer-Verlag: Berling, **2003**.

Graphical Abstract Image